BUTTERWORTH HEINEMANN

*Polymer* Vol. 36 No. 4. pp. 699-706, 1995
Copyright © 1995 Elsevier Science Ltd
Printed in Great Britain. All rights reserved
0032-3861/95/$10.00 + 0.00

# Structure and molecular motion changes in poly(ethylene terephthalate) induced by annealing under dry and wet conditions

**Tamako Toda***
*Showa Women's Junior College, Tokyo 154, Japan*

**and Hirohisa Yoshida**
*Department of Industrial Chemistry, Tokyo Metropolitan University, Tokyo 192-03, Japan*

**and Koushi Fukunishi**
*Department of Chemistry and Materials Technology, Kyoto Institute of Technology, Kyoto 606, Japan*
*(Received 3 June 1994; revised 2 September 1994)*

Structural changes in poly(ethylene terephthalate) (PET) induced by annealing under dry nitrogen gas flow (dry annealing) and in water (wet annealing) were investigated using small- and wide-angle X-ray diffraction methods, density measurements, differential scanning calorimetry and dynamic viscoelastic measurements. The degree of crystallinity of PET was evaluated by wide-angle X-ray diffraction patterns and by heat of fusion measured using differential scanning calorimetry. Based on the two-phase concept, the amorphous density of PET was calculated from the observed density and degree of crystallinity. The amorphous density decreased as crystallization increased for both the dry and wet conditions. The glass transition temperature and activation energy of the glass transition of PET based on dynamic viscoelastic measurements decreased as crystallization proceeded. Since the amorphous density decreased with annealing in the late phases of crystallization, molecular motion in the amorphous region easily occurred as crystallization proceeded. Water molecules enhanced the structural changes during the crystallization of PET.

**(Keywords: poly(ethylene terephthalate); structural parameters; annealing-induced changes)**

## INTRODUCTION

From studies of the photofading behaviour of dyes in polymer substrates[1-9], it is known that the fading behaviour is affected by the physical state, such as aggregation state, of dyes attributable to the morphological characteristics of the polymer. We studied the dispersion state of dyes in poly(ethylene terephthalate) (PET) by microspectrophotometry[10] and estimated the physical state of dyes in PET using the interaction parameter of Flory's equation[11]. It was found that monodisperse dyes and aggregated dyes coexisted in PET[10,11]. Further, the effects of dyes and absorbed water on the molecular motion of PET were discussed based on its dynamic viscoelastic property. Both dyes and absorbed water enhanced the segmental mobility of PET as a result of their plasticizing effect[12]. It is expected that the physical state and movement of dyes and absorbed water are strongly affected by the amorphous structure and molecular mobility of the polymer matrix. In this way, the physical state of absorbed low-molecular-weight molecules is considered to correlate strongly with the amorphous structure of PET. In other words, information on the structural change in the amorphous region of PET induced by small molecules might be useful for the clarification of the physical state of the molecules. In this study, water is employed as a candidate for small molecules, and the structural change in the amorphous region of PET induced by annealing under dry and wet conditions is discussed in terms of molecular motion in the amorphous state and dyeing behaviour.

Structure and property changes in PET caused by annealing have been reported for the bulk and highly oriented states using electron microscopy[13-15], wide-angle and small-angle X-ray diffraction methods[14-20], density measurements[15,19], differential scanning calorimetry[15,19,21-23], infra-red absorption spectroscopy[24,25], dynamic viscoelastic measurements[26,27] and microhardness[28,29]. Wide-angle X-ray diffraction (WAXD) is directly related to order and disorder of the polymers, hence to crystallinity. Based on the two-phase concept, various procedures using both absolute and relative methods have been reported that evaluate the degree of crystallinity from a WAXD profile[30,31]. In addition to the WAXD method, the degree of crystallinity of PET is evaluated by density, infra-red absorption spectra and differential scanning calorimetry (d.s.c.). Usually, the

* To whom correspondence should be addressed

degree of crystallinity obtained from the density shows good agreement with that obtained from WAXD methods. According to Fontaine *et al.*[19], the values obtained by an absolute crystallinity method from WAXD profiles show good agreement with the values obtained from the density. However, these values differ from the degree of crystallinity calculated from the heat of fusion for PET annealed at various temperatures. Groeninckx *et al.*[15] also reported a large discrepancy between the crystallinities of PET obtained from density measurements and from the heat of fusion measured by d.s.c. The obtained crystallinity contains some errors in each method, such as the effect of crystallite orientation for the WAXD method, the effect of free energy of the crystal surfaces for the d.s.c. method, and the assumption of constant densities of the crystalline and amorphous states for the density method.

In this study, the changes in various parameters characterizing semicrystalline PET, such as the degree of crystallinity obtained by various methods, the long spacing and the amorphous structure, caused by annealing are also investigated. The parameters and the amorphous structure are compared with the molecular mobility of the amorphous state.

## EXPERIMENTAL

### *Sample*

An extruded PET, a 9 $\mu$m thick film, manufactured by Teijin Co. Ltd, was used throughout the experiments. Preliminary WAXD work suggested that the original PET film was a highly crystallized sample in which the *b* axis was fully oriented parallel to the film surface. The density of the original PET was 1.4015 g cm$^{-3}$ at 23°C. PET samples were annealed at various temperatures from 120 to 210°C for 1 h under a dry nitrogen gas atmosphere (dry annealing) and in water (wet annealing). All annealed samples were optically clear. After annealing, PET samples were cooled to room temperature and stored in a desiccator over diphosphorus pentaoxide.

### *Dye sorption*

PET films were dyed with $1.754 \times 10^{-4}$ mol l$^{-1}$ of crystal violet chloride (C.I. Basic Violet 3) (CV) solution at 130°C for 2 h in a liquor ratio of 1250:1 under pressure. All dyed films were successively washed with water and ethanol in order to remove any excess dye on the film surface and then air dried at room temperature. The adsorbed dye was extracted with ethanol and the dye concentration was determined using a spectrophotometric method[9].

### *Density measurement*

PET densities were measured in a density gradient column consisting of n-heptane and carbon tetrachloride at 23 ± 0.1°C. At each annealing condition, the densities of at least three different species were measured. The optimum immersion time was selected from the relationship between the apparent density and the square root of the immersion time. The volume degree of crystallinity from the density ($X_d$) was calculated assuming a crystal density value of $\rho_c = 1.4895$ g cm$^{-3}$ and an amorphous density value of $\rho_a = 1.3379$ g cm$^{-3}$ (refs. 28, 29) using the following equation:

$$X_d = \rho_c(\rho - \rho_a)/\rho(\rho_c - \rho_a) \quad (1)$$

### *X-ray diffraction measurements*

WAXD profiles of PET were measured using a Mac Science model SRA MXP-18 X-ray instrument operating at 40 kV, 300 mA. Monochromated X-ray radiation was used and the X-ray wavelength was 0.154 05 nm. A WAXD profile was detected in both the reflection and transmission modes using a scintillation counter in conjunction with a pulse-height analyser. In order to eliminate the surface orientation effect of crystallites, the sample was wound tightly and attached to a fibre sample holder to determine the degree of crystallinity in the transmission mode. Samples were rotated at 10 rev min$^{-1}$ during the measurements in order to eliminate the biaxial orientation effect, and a radial diffractometer scanned in the $2\theta$ range from 5 to 60° in the step-scanning mode. The raw data were subjected to background subtraction, and to polarization, absorption and incoherent scattering corrections.

Small-angle X-ray scattering (SAXS) profiles were measured using SAXS optics installed at BL-10C at the Photon Factory of the National Laboratory for High Energy Physics, Tsukuba, Japan. The X-ray wavelength was selected using a double crystal monochrometer and was fixed at 0.1488 nm. A camera length of 2.0 m was used to examine the scattering profile, which was recorded using a unidirectional position-sensitive proportional photon counter with a 600 s exposure time. The SAXS profiles were observed in the transmission mode over scattering vectors $s = 2 \sin\theta/\lambda$ in the range $8 \times 10^{-3}$ nm$^{-1}$ $< s < 0.3$ nm$^{-1}$. The raw data were subjected to background subtraction and to an absorption correction.

### *Thermal analysis*

Thermal properties of PET were measured using a Seiko differential scanning calorimeter DSC 200 connected to a Seiko thermal analysis system SSC 5000 equipped with a cooling apparatus. The d.s.c. heating curve was measured at 10°C min$^{-1}$ in the temperature range from 0 to 300°C under dry nitrogen gas flow. The sample weight was about 4 mg. Temperature and enthalpy were corrected using pure indium and tin. The melting peak temperature was evaluated as a melting temperature ($T_m$). The degree of crystallinity is also evaluated from the heat of fusion measured by d.s.c. ($X_{dsc}$). This method is based on a thermodynamic definition of order and it requires the absolute value of the heat of fusion of the fully crystalline polymer, $\Delta H_{m0} = 119.8$ J g$^{-1}$ (ref. 30). $X_{dsc}$, expressed as a weight fraction, can be determined as follows:

$$X_{dsc} = \Delta H_{m,obs}/\Delta H_{m0} \quad (2)$$

The dynamic viscoelastic properties of PET were measured using a Seiko dynamic mechanical spectrometer DMS 200 connected to a Seiko material analysis station MAS 5700. Dynamic viscoelastic spectra were measured in the tension mode at 0.1, 0.2, 0.5, 1, 2, 5 and 10 Hz in the temperature range from 23 to 200°C heated at 1°C min$^{-1}$.

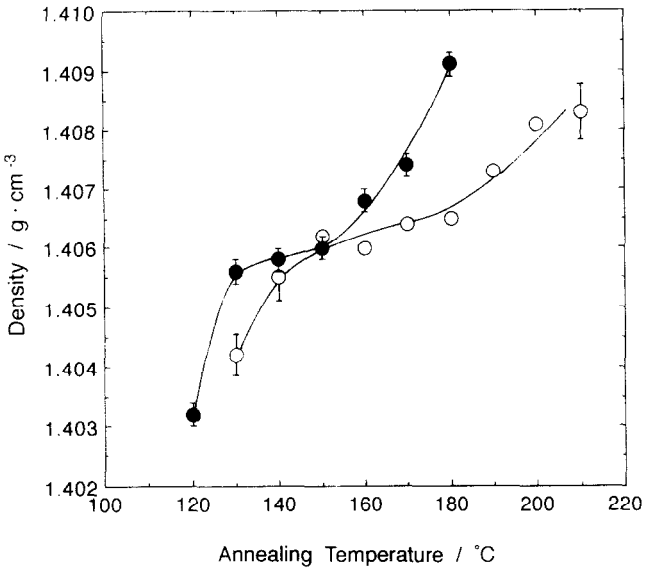


**Figure 1** Density changes with annealing temperature for PET annealed under dry (○) and wet (●) conditions

## RESULTS AND DISCUSSION

### *Density*

*Figure 1* shows the changes in density of PET annealed under the dry and wet conditions as a function of annealing temperature. All samples were annealed for 1 h at each annealing temperature. Further annealing caused a small increase in density for all annealing temperatures. Annealing temperatures were classified into three regions using the measured density of PET: below 1.405 g cm$^{-3}$, between 1.405 and 1.406 g cm$^{-3}$ and above 1.406 g cm$^{-3}$, for both annealing conditions. Density significantly increased from 1.4015 to 1.4055 g cm$^{-3}$ with annealing; however, the density changed slightly from 1.4055 to 1.4065 g cm$^{-3}$ even if the annealing temperature increased. The density then increased again from annealing temperatures above 190°C for the dry condition and above 180°C for the wet condition. A similar change in density occurred for the wet annealing condition at a lower annealing temperature as compared to the dry annealing condition. The density of the wet annealed PET was higher than that of the dry annealed PET under all annealing conditions. Crystallization from the glassy state occurs in the temperature range above the glass transition temperature. The degree of PET crystallinity increases from 0 to 30% in the temperature range between 110 and 120°C, and increases gradually with an increase in annealing temperature up to 230°C[28]. It has been reported that PET crystallized at high $T$ ($T > 200$°C) exhibits a very well developed lamellar morphology within the spherulites and, as a consequence, can be analysed within the frame of the two-phase concept[15].

### *Dye sorption*

It is known that dye exhaustion of heat-set PET fibres changes with annealing temperature[32–38]. Although this was considered to be due to the fine structure of the PET fibre, the details are still not clear. *Figure 2* shows the changes in dye exhaustion of PET annealed under dry and wet conditions in relation to the annealing temperature. The amount of dye sorbed increased with increasing annealing temperature. The ratio of the absorbance of the $\alpha$ band to that of the $\beta$ band in the CV spectra has been used as an indication of the degree of aggregation of the dye. The value of $\alpha/\beta$ ratio decreased with an increase in dye exhaustion of PET. This result is due to dye–dye aggregation[11]. Equilibrium sorption was not established after long-term dyeing, but the films that were annealed under the wet condition or at high temperature were degraded into pieces. These results suggest that the amorphous state of PET may change with crystallization, since the dye molecules are sorbed in only the amorphous region.

### *Structural change of crystalline region*

Since the original sample showed high crystallinity, a slight difference was observed in the WAXD profiles of the original and annealed PET films. WAXD profiles of the original and annealed PET showed a diffraction peak of the (100) plane in the reflection mode; however, WAXD profiles of the stacked films measured in the transmission mode showed the diffraction peak of the (010) plane instead of the (100) plane. This fact suggested that the $b$ axis of the crystallite was fully aligned parallel to the film surface. On the other hand, WAXD profiles of the wound films showed both diffraction peaks of the (100) and the (010) planes. The intensity distribution of the diffraction peak from the (010) plane, which was observed by rotating the sample at a fixed $2\theta$, suggested a weak biaxial orientation of the crystallite. In order to determine the crystallinity of the highly oriented system, the absolute method proposed by Ruland[31] is not suitable. We used the following relative method[39] to evaluate the degree of crystallinity from the WAXD profiles.

The amorphous standard PET was prepared by quenching from the molten state. The WAXD profiles were separated into contributions from the amorphous and crystalline regions. Since we assumed that no diffraction peaks existed in the $2\theta$ range below 14°, the WAXD profile of the amorphous standard was multiplied by a constant value in order to make the intensity at $2\theta = 14°$ equal, and then the above profile was subtracted

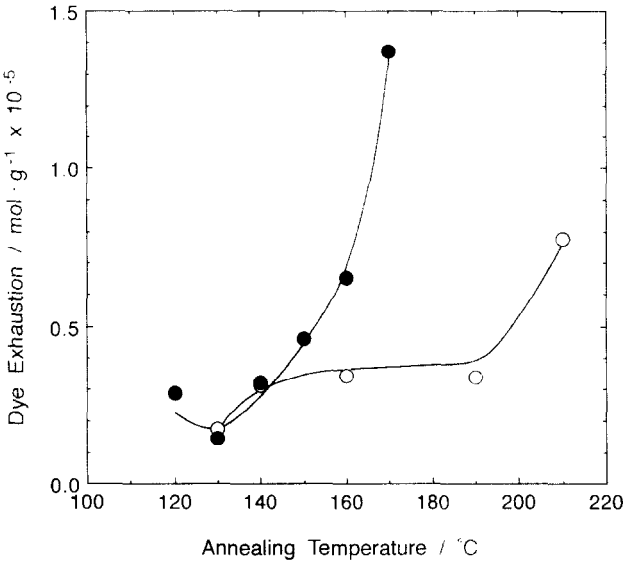


**Figure 2** Dye exhaustion changes with annealing temperature for PET annealed under dry (○) and wet (●) conditions

**Table 1** Physical properties of PET annealed under dry condition

| Annealing temperature (°C) | Density at 23 °C (g cm$^{-3}$) | Degree of crystallinity | | | | Thermal properties | | | | Crystal size | | Long period |
|---|---|---|---|---|---|---|---|---|---|---|---|---|
| | | $X_{c,r}$[a] | $X_{c,t}$[b] | $X_d$[c] | $X_{dsc}$[a] | $T_{m1}$[e] (°C) | $T_{m2}$[f] (°C) | $\Delta H_{m1}$[g] (J g$^{-1}$) | $\Delta H_{m2}$[h] (J g$^{-1}$) | $D_{100}$[i] (nm) | $D_{010}$[j] (nm) | $L$ (nm) |
| Original | 1.4015 | 0.630 | 0.341 | 0.446 | 0.398 | | 256.6 | 0 | 47.7 | 6.9 | 7.7 | 14.8 |
| 130 | 1.4042 | 0.629 | 0.386 | 0.464 | 0.396 | 135.0 | 256.6 | 0.6 | 46.8 | 6.8 | 8.3 | 14.7 |
| 140 | 1.4055 | 0.631 | 0.416 | 0.473 | 0.405 | 139.0 | 256.4 | 0.85 | 47.7 | 6.6 | 8.6 | 14.7 |
| 150 | 1.4062 | 0.625 | 0.420 | 0.477 | | | | | | | | |
| 160 | 1.4060 | 0.640 | 0.426 | 0.476 | 0.403 | 156.0 | 256.5 | 1.1 | 47.1 | 6.9 | | 14.8 |
| 170 | 1.4064 | 0.645 | 0.427 | 0.479 | 0.407 | 159.0 | 256.4 | 1.4 | 47.4 | 7.2 | 9.3 | 14.8 |
| 180 | 1.4065 | 0.642 | 0.438 | 0.479 | 0.397 | 182.0 | 256.4 | 1.2 | 46.4 | 6.6 | 9.4 | 14.7 |
| 190 | 1.4073 | 0.646 | 0.440 | 0.485 | 0.395 | 192.0 | 256.4 | 1.1 | 46.2 | 7.4 | | 14.9 |
| 200 | 1.4081 | 0.649 | 0.458 | 0.490 | 0.409 | 197.0 | 256.4 | 1.5 | 48.5 | 7.0 | 9.3 | 15.1 |
| 210 | 1.4083 | 0.650 | 0.572 | 0.491 | 0.533 | 207.0 | 256.2 | | 63.9 | 6.9 | 9.7 | 15.1 |

[a] Obtained from WAXD profiles in reflection mode
[b] Obtained from WAXD profiles in transmission mode
[c] Obtained from density
[d] Obtained from melting enthalpy ($\Delta H_{m1} + \Delta H_{m2}$)
[e] Observed at lower temperature
[f] Observed at higher temperature
[g] Observed at lower temperature
[h] Observed at higher temperature
[i] Along $a$ axis
[j] Along $b$ axis

**Table 2** Physical properties of PET annealed under wet condition[a]

| Annealing temperature (°C) | Density at 23 °C (g cm$^{-3}$) | Degree of crystallinity | | | | Thermal properties | | | | Crystal size | | Long period |
|---|---|---|---|---|---|---|---|---|---|---|---|---|
| | | $X_{c,r}$ | $X_{c,t}$ | $X_d$ | $X_{dsc}$ | $T_{m1}$ (°C) | $T_{m2}$ (°C) | $\Delta H_{m1}$ (J g$^{-1}$) | $\Delta H_{m2}$ (J g$^{-1}$) | $D_{100}$ (nm) | $D_{010}$ (nm) | $L$ (nm) |
| 120 | 1.4032 | 0.642 | 0.423 | 0.457 | 0.407 | 132.2 | 256.6 | 0.9 | 47.8 | 7.1 | 8.9 | 15.2 |
| 130 | 1.4056 | | 0.482 | 0.473 | 0.412 | 146.5 | 256.9 | 1.1 | 48.2 | 6.6 | | 15.2 |
| 140 | 1.4058 | 0.650 | 0.505 | 0.475 | 0.424 | 149.8 | 256.9 | 1.4 | 49.4 | 7.4 | 9.3 | 15.5 |
| 150 | 1.4060 | 0.661 | 0.522 | 0.476 | 0.424 | 169.0 | 257.3 | 0.9 | 49.9 | 7.3 | 10.0 | 15.6 |
| 160 | 1.4068 | 0.660 | 0.539 | 0.481 | 0.452 | 172.7 | 257.7 | 1.2 | 53.0 | 7.8 | 10.2 | 15.7 |
| 170 | 1.4074 | 0.668 | 0.571 | 0.485 | 0.426 | 184.0 | 257.4 | 0.8 | 50.3 | 6.9 | 10.0 | 15.8 |
| 180 | 1.4091 | 0.670 | 0.561 | 0.497 | 0.451 | 194.5 | 258.0 | 0.85 | 53.2 | 7.5 | | |

[a] See footnote to *Table 1* for more details about symbols used

from the sample. The ratio between integral intensity of the crystalline contribution and total integral intensity gave the degree of crystallinity ($X_c$) expressed as a weight fraction. This relative method was applied to WAXD profiles obtained in both the reflection and transmission modes. The values of $X_c$ obtained from the reflection WAXD ($X_{c,r}$) and from the transmission WAXD ($X_{c,t}$) are listed in *Table 1* (dry annealing condition) and *Table 2* (wet annealing condition). The crystallinity values evaluated from the density ($X_d$) and from the d.s.c. ($X_{dsc}$) are also listed in *Tables 1* and *2*.

*Figures 3* and *4* show changes in crystallinity evaluated from various methods with annealing temperature for PET annealed under the dry and wet conditions, respectively. The degree of crystallinity ($X_c$) evaluated from the reflection mode ($X_{c,r}$) was almost constant or increased slightly with increasing annealing temperature for both the dry and wet conditions. On the other hand, $X_c$ evaluated from the transmission mode ($X_{c,t}$) significantly increased with an increase in annealing temperature for the wet annealed PET; however, the $X_c$ of the dry annealed PET increased slightly in the temperature

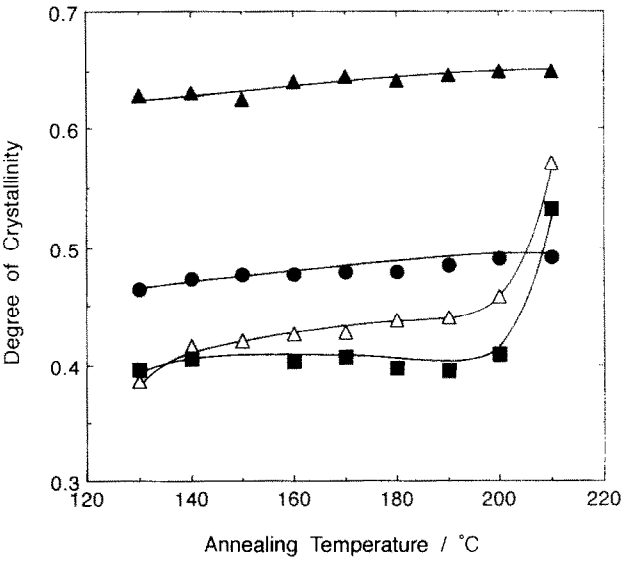


**Figure 3** Changes in crystallinity evaluated by reflection WAXD ($X_{c,r}$, ▲), transmission WAXD ($X_{c,t}$, △), density ($X_d$, ●) and d.s.c. ($X_{dsc}$, ■) for PET annealed under dry conditions

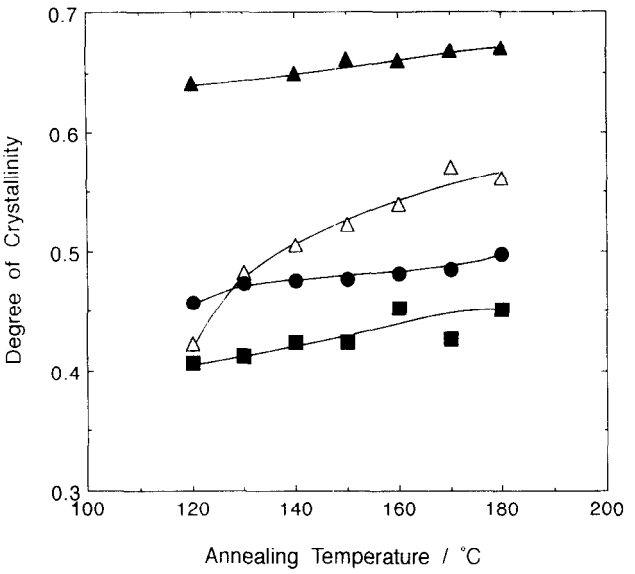


**Figure 4** Changes in crystallinity evaluated by reflection WAXD ($X_{c,r}$, ▲), transmission WAXD ($X_{c,t}$, △), density ($X_d$, ●) and d.s.c. ($X_{dsc}$, ■) for PET annealed under wet conditions

range below 200°C. $X_c$ evaluated from the transmission WAXD of dry annealed PET changed like the density change of the dry annealed PET shown in *Figure 1*. The values of $X_{c,t}$ were almost the same as $X_{dsc}$ for the dry annealed PET; however, a discrepancy among the values evaluated by various methods was observed for the wet annealed PET (*Figure 4*).

Annealed PET samples showed two endothermic peaks in the heating d.s.c. curve. The temperature of the lower melting peak ($T_{m1}$), the temperature of the higher melting peak ($T_{m2}$) and the heat of fusion obtained for both endothermic peaks ($\Delta H_{m1}$, $\Delta H_{m2}$) are listed in *Tables 1* and *2*. For the dry annealed PET, $T_{m2}$ remained constant over all annealing temperature ranges, whereas $T_{m1}$ depended strongly on the annealing temperature and was almost the same as the annealing temperature. In the case of the wet condition, however, both $T_{m1}$ and $T_{m2}$ depended strongly on annealing temperature. The changes in $\Delta H_{m2}$ showed the same tendency as the $T_{m2}$ change for both the dry and wet annealed PET. The entropy change ($\Delta S_m$) values at melting calculated from $\Delta H_{m2}$ and $T_{m2}$ were almost the same for both annealing conditions except for the sample dry annealed at 210°C whose higher melting peak overlapped with the lower melting peak. This fact suggested that the increase in $T_m$ was caused by the increase in crystal size.

The positions of diffraction peaks of the (100) and (010) planes scarcely changed by annealing under both conditions. From the half-width of the diffraction peaks of the (100) and (010) planes, the crystal sizes along the $a$ and $b$ axes, respectively, were estimated using Scherrer's equation:

$$D = 0.94\lambda / \Delta x \cos\theta \qquad (3)$$

Here, the $D$ and $\Delta x$ are crystal sizes along the $i$ axis and half-width of the diffraction peak in radians, respectively. The obtained values of crystal size along the $a$ and $b$ axes are listed in *Tables 1* and *2*. Although the crystal size along the $a$ axis ($D_{100}$) showed some scatter, the $D_{100}$ values were almost the same or increased slightly with an increase in annealing temperature. The crystal size along the $b$ axis ($D_{010}$) increased with an increase in annealing temperature for both annealing conditions. The values of $D_{010}$ of wet annealed PET were larger than those of dry annealed PET. The values of $D_{100}$ and $D_{010}$ contained some error, because Scherrer's equation scarcely considered the effect of crystal lattice irregularities. However, these observations were compatible with the change in $X_c$ evaluated from the reflection and transmission modes.

From the maxima of the SAXS profile, the long period was calculated using Bragg's law. *Figure 5* shows the changes in the long period as a function of annealing temperature for PET annealed under dry and wet conditions. The long period of the dry annealed PET increased slightly with an increase in annealing temperature. However, the long period of the wet annealed PET increased more steeply than that of the dry annealed PET. The long period of the wet annealed PET was larger than that of the dry annealed PET for all annealing temperatures. As well as slight increases in the crystal size along the $a$ and $b$ axes, the thickening of the lamellae occurred due to annealing. The lamellar thickening easily occurred in the case of annealing under wet condition.

*Structural change in amorphous region*

As previously described, the amount of dye absorbed in PET increased with an increase in the total density of PET. This fact suggests that the structure of the amorphous region of PET changed during crystallization induced by annealing. In the case of semicrystalline polymers, the high-order structure is considered by the two-phase concept and the three-phase concept including an intermediate phase such as paracrystal phase[40], condis crystal[41] and interphase[42]. The paracrystalline phase transforms to the triclinic crystal when PET is annealed at a temperature above 100°C[20]. As no paracrystalline reflections are observed in WAXD profiles of PET annealed under both conditions, we employed the two-phase concept to analyse amorphous structure. The unit-cell dimensions of PET crystal and crystal density change by annealing[43,44]. As described above, however,

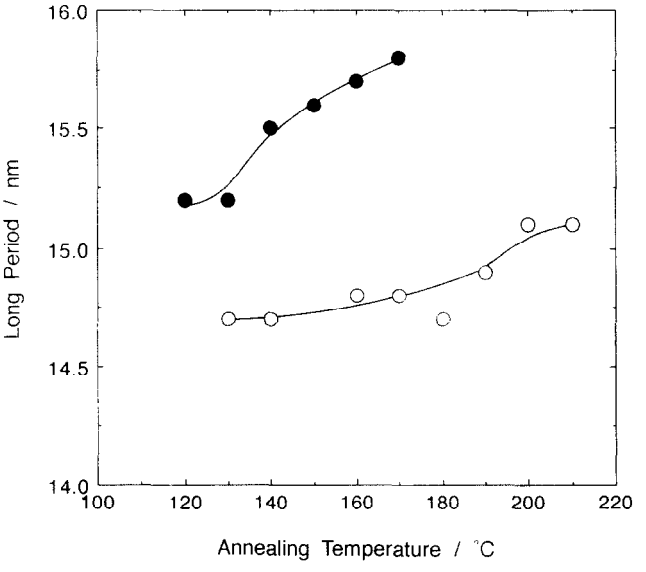


**Figure 5** Long-period changes with annealing temperature for PET annealed under dry (○) and wet (●) conditions

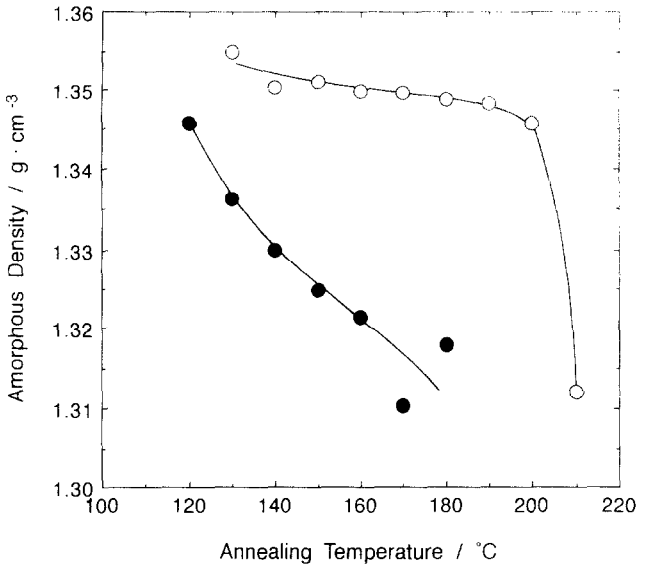


**Figure 6** Changes in amorphous density with annealing temperature for PET annealed under dry (○) and wet (●) conditions

because the positions of diffraction peaks of the (010) and the (100) planes scarcely changed by annealing, we expected the constancy of the crystal density. From the observed values of density and crystallinity evaluated from the transmission WAXD, the amorphous density was calculated assuming a constant density of the crystalline region ($\rho_c = 1.4895\,g\,cm^{-3}$) (refs. 28, 29). The calculated values of the amorphous density of PET annealed under dry and wet conditions are plotted in *Figure 6*. The obtained values of the amorphous density for the dry annealed PET were comparable with previously reported values ($\rho_a = 1.3379\,g\,cm^{-3}$ (refs. 28, 29), $\rho_a = 1.335\,g\,cm^{-3}$ (ref. 15)). However, the values for the wet annealed PET were lower than the reported values. The calculated amorphous density decreased with an increase in annealing temperature for both conditions. At a given annealing temperature, the amorphous density of the wet annealed PET was lower than that of the dry annealed PET.

In the SAXS measurement, not only the long period but also the scattering intensity increased with an increase in annealing temperature for both the dry and wet annealing conditions. In an isotropic two-phase system, the principle of conservation of scattered intensity can be written as the following equation[45]:

$$4\pi \int_0^{\infty} s^2 I(s)\,ds = V(\rho_1 - \rho_2)^2 v_1(1 - v_1) \qquad (4)$$

where $s$ is related to the scattering angle $2\theta$ and the incident wavelength $\lambda$ by $s = 2\sin\theta/\lambda$, $I(s)$ is the absolute scattering intensity at a particular value of $s$, $V$ is the irradiated volume, $\rho_1$ and $\rho_2$ are the electron densities of the crystalline and amorphous phases present, respectively, and $v_1$ is the volume fraction of the crystalline phase. Owing to the limitations in the $s$ region, equation (4) is replaced by the following equation using the intensity of the scattering peak integrating $s$ from $0.03\,nm^{-1}$ to $0.16\,nm^{-1}$ ($Q$) and the densities of the crystalline and amorphous regions ($\rho_c$, $\rho_a$):

$$Q \propto (\rho_c - \rho_a)^2 \qquad (5)$$

*Figure 7* shows the relationship between $Q$ and the annealing temperature for PET annealed under dry and wet conditions. The $Q$ values increased with an increase in annealing temperature for both the dry and wet annealed conditions. The values of $Q$ for the wet annealed PET were larger than those of the dry annealed PET. Although the $Q$ values have not been normalized by the volume fraction of the crystalline phase, these facts suggest that the density difference between the crystalline phase and amorphous region increased with an increase in annealing temperature. Assuming a constant crystalline density, the amorphous density should decrease with an increase in annealing temperature. As previously mentioned, a large structural change occurred when PET was annealed under wet conditions. The lamellar thickening easily occurred and $T_{m2}$ increased with an increase in annealing temperature. These results could be explained by the suggestion of Hatakeyama *et al.*[46] that water molecules tightly attached to the amorphous PET chain induce a molecular rearrangement in the short-range order of the glassy chain.

*Molecular motion at glass transition*

Dynamic viscoelastic spectra of annealed PET showed two relaxation peaks at around −50°C ($\beta$ relaxation) and 100°C ($\alpha$ relaxation), which were assigned to local-mode relaxation and glass transition, respectively[47]. If the amorphous density decreased with the increase in annealing temperature, the molecular motions in the amorphous region may be influenced by the annealing conditions. *Figure 8* shows the effect of annealing temperature on the dynamic loss modulus ($E''$) peak temperature of the $\alpha$ relaxation measured at 10 Hz. The $E''$ peak temperature of both the dry and wet annealed PET decreased with an increase in annealing temperature. In other words, the glass transition temperature decreased as crystallization proceeded. As opposed to the results shown in *Figures 6* and *7*, the glass transition temperature of the wet annealed PET showed almost the same tendency as the dry annealed PET. The reason for this fact is that the segmental motion of the polymer chain is restricted, since the molecular chains in the amorphous

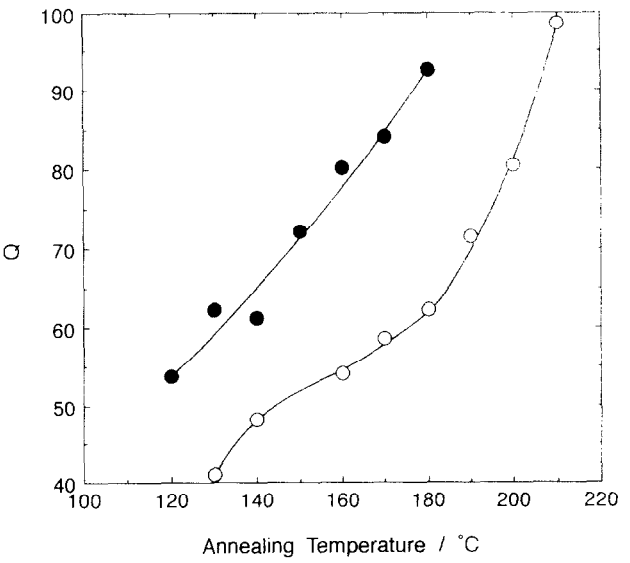


**Figure 7** Relationship between $Q$ and annealing temperature for PET annealed under dry (○) and wet (●) conditions

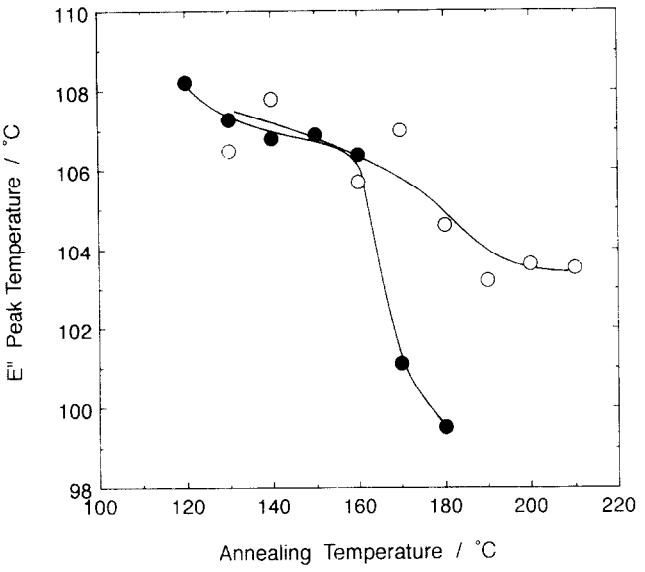


**Figure 8** Changes in dynamic loss modulus ($E''$) peak temperature of $\alpha$ relaxation measured at 10 Hz for PET annealed under dry (○) and wet (●) conditions as a function of annealing temperature

**Table 3** Dynamic viscoelastic properties of $\alpha$ relaxation of PET annealed under dry condition

| Annealing temperature (°C) | Dynamic loss temperature (°C) | | | Activation energy (kJ mol$^{-1}$) | $\Delta E/E'(\infty)$ |
|---|---|---|---|---|---|
| | 1 Hz | 10 Hz | 100 Hz | | |
| 130 | 100.7 | 106.5 | 111.1 | 394.7 | 0.272 |
| 140 | 100.8 | 107.8 | 112.4 | 415.2 | 0.257 |
| 150 | | | | | |
| 160 | 98.8 | 105.7 | 111.5 | 377.5 | 0.237 |
| 170 | 100.8 | 107.0 | 112.5 | 355.7 | 0.233 |
| 180 | 98.8 | 104.6 | 112.7 | 364.1 | 0.235 |
| 190 | 97.4 | 103.2 | 110.3 | 372.0 | 0.222 |
| 200 | 96.7 | 103.6 | 109.4 | 345.3 | 0.217 |
| 210 | 96.5 | 103.5 | 111.6 | 320.5 | 0.204 |

**Table 4** Dynamic viscoelastic properties of $\alpha$-relaxation of PET annealed under wet condition

| Annealing temperature (°C) | Dynamic loss temperature (°C) | | | Activation energy (kJ mol$^{-1}$) | $\Delta E/E'(\infty)$ |
|---|---|---|---|---|---|
| | 1 Hz | 10 Hz | 100 Hz | | |
| 120 | 103.5 | 108.2 | 114.0 | 418.0 | 0.263 |
| 130 | 101.5 | 107.3 | 113.1 | 382.2 | 0.263 |
| 140 | 100.9 | 106.8 | 113.7 | 378.5 | 0.254 |
| 150 | 101.1 | 106.9 | 112.7 | 394.0 | 0.243 |
| 160 | 99.4 | 106.4 | 113.3 | 378.3 | 0.222 |
| 170 | 93.0 | 101.1 | 109.2 | 345.5 | 0.210 |
| 180 | 92.0 | 99.5 | 108.2 | 342.0 | 0.188 |

region almost link with the molecular chains in the crystalline region.

From the frequency dependence of the loss peak temperature observed by the dynamic relaxation measurements, the apparent activation energy ($E^*$) of the relaxation process was evaluated by the following equation:

$$E^* = -R\,\mathrm{d}(\ln \tau^{-1})/\mathrm{d}(1/T) = -R\,\mathrm{d}(\ln f)/\mathrm{d}(1/T) \quad (6)$$

Here, $R$, $\tau$, $f$ and $T$ are the gas constant, relaxation time, measuring frequency and peak temperature of tan $\delta$ peak observed at a given frequency, respectively. The peak temperature of the dynamic loss peak observed at 1, 10 and 100 Hz and the calculated apparent activation energy for the $\alpha$ relaxation are listed in *Table 3* (dry annealing condition) and *Table 4* (wet annealing condition). The $E^*$ values show some scatter; however, $E^*$ decreases with an increase in annealing temperature for both annealing conditions. The changes in the glass transition temperature and activation energy of the $\alpha$ relaxation with annealing temperature suggested that molecular motion in the amorphous region easily occurred as the crystallization proceeded. This fact also suggested that the amorphous density decreased with an increase in annealing temperature.

From the temperature dispersion spectra of the dynamic viscoelasticity, the relaxation strength ($\Delta E$) is obtained using the following equation:

$$\Delta E = (2/\pi)\int_{-\infty}^{\infty} E''(f\tau)\,\mathrm{d}\log f = (2E^*/\pi R)\int_{0}^{\infty} E''(T)\,\mathrm{d}(1/T) \quad (7)$$

Here, $f$, $\tau$ and $E^*$ are frequency, relaxation time and activation energy, respectively. According to Yamafuji[48], the relaxation strength is proportional to the number of molecules responsible for the observed relaxation. The obtained values of the relaxation strength of the $\alpha$ relaxation are shown in *Figure 9* for PET annealed under dry and wet conditions. The relaxation strength decreased with an increase in annealing temperature. These facts suggested that the number of molecules responsible for the glass transition decreased with an increase in annealing temperature. In other words, the amorphous density decreased as crystallization proceeded and the decreasing ratio of the amorphous density for the wet annealed PET was larger than that for the dry annealed PET.

## CONCLUSIONS

The degree of crystallinity increased with an increase in annealing temperature and a remarkable increase in

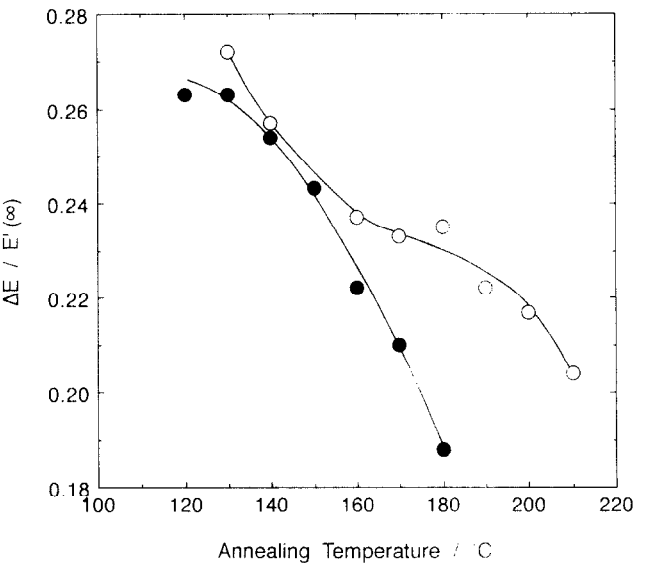


**Figure 9** Changes in relaxation intensity with annealing temperature for PET annealed under dry (○) and wet (●) conditions

crystallinity was observed under wet annealing conditions. For dry annealed PET, $T_{m2}$ remained constant over the entire annealing temperature range; however, $T_{m2}$ of the wet annealed PET strongly depended on the annealing temperature. The long period and crystal size increased with an increase in annealing temperature for both annealing conditions; especially, the wet annealed PET showed a large increase in lamellar thickness and crystal size. The amorphous density of the wet annealed PET significantly decreased with an increase in annealing temperature. The amorphous structure changed as a result of the plasticizing effect of the absorbed water in the amorphous region of PET under wet annealing conditions. The sparse amorphous structure of the wet annealed PET caused a segmental motion of PET in the amorphous region. The decrease in amorphous density of PET with crystallization completely explained the glass transition and dye absorption behaviours.

## REFERENCES


1 Baxter, G., Giles, C. H., Mckee, M. N. and Macaulay, N. *J. Soc. Dyers Colour.* 1955, **71**, 386
2 Weissbein, L. and Coven, G. E. *Text. Res. J.* 1960, **30**, 62
3 Giles, C. H. and Rahman, S. M. K. *Text. Res. J.* 1961, **31**, 1012
4 Giles, C. H., Hojiwala, B. J. and Shah, C. D. *J. Soc. Dyers Colour.* 1972, **88**, 403
5 Hida, M., Okabayashi, M. and Yabe, A. *Kogyo Kagaku Zasshi* 1969, **72**, 265
6 Suganuma, K., Hida, M. and Yabe, A. *Sen-i Gakkaishi* 1979, **35**, T-388
7 Nakamura, R. and Hida, M. *Sen-i Gakkaishi* 1983, **39**, T-125
8 Toda, T. and Hida, M. The 30th Symposium on Dyeing Chemistry, Reprints, 1988, p. 84
9 Toda, T. and Hida, M. *Sen-i Gakkaishi* 1990, **46**, 155
10 Ohtsu, T., Nishida, K., Nagumo, K. and Tsuda, K. *Colloid Polym. Sci.* 1974, **252**, 377
11 Toda, T., Yoshida, H. and Hida, M. *Sen-i Gakkaishi* 1993, **49**, 237
12 Toda, T., Yoshida, H. and Hida, M. *Sen-i Gakkaishi* 1992, **48**, 84
13 Yeh, G. S. Y. and Geil, P. H. *J. Macromol. Sci. (B)* 1967, **1**, 235
14 Fischer, E. W. and Fakirov, S. *J. Mater. Sci.* 1976, **11**, 1041
15 Groeninckx, G., Reynaers, H., Berghans, H. and Smets, G. *J. Polym. Sci., Polym. Phys. Edn.* 1980, **18**, 1311
16 Lemanska, G. and Narebska, A. *J. Polym. Sci., Polym. Phys. Edn.* 1980, **18**, 917
17 Dumbleton, J. H. *J. Polym. Sci. (A-2)* 1969, **7**, 667
18 Elsner, G., Koch, M. H. J., Bordas, J. and Zachmann, H. G. *Makromol. Chem.* 1981, **182**, 1263
19 Fontaine, F., Ledent, J., Groeninckx, G. and Reynaers, H. *Polymer* 1982, **23**, 185
20 Asano, T. and Seto, T. *Polym. J.* 1973, **5**, 72
21 Fakirov, S., Fischer, E. W., Hoffmann, R. and Schmidt, G. F. *Polymer* 1977, **18**, 1121
22 Roberts, R. C. *Polymer* 1969, **10**, 113
23 Deopura, B. L., Kumar, V. and Shiha, T. B. *Polymer* 1977, **18**, 856
24 Miller, R. G. J. and Wills, H. A. *J. Polym. Sci.* 1956, **19**, 485
25 Farrow, G. and Word, I. M. *Polymer* 1960, **1**, 330
26 Pinnock, P. R. and Ward, I. M. *Polymer* 1966, **7**, 255
27 Samuels, R. J. *J. Polym. Sci. (A-2)* 1972, **10**, 781
28 Santa Cruz, C., Balta Calleja, F. J., Zachmann, H. G., Stribeck, N. and Asano, T. *J. Polym. Sci., Polym. Phys. Edn.* 1991, **29**, 819
29 Balta Calleja, F. J., Santa Cruz, C. and Asano, T. *J. Polym. Sci., Polym. Phys. Edn.* 1993, **31**, 557
30 Wunderlich, B. 'Macromolecular Physics', Academic Press, New York, 1973, Vol. 1, p. 389
31 Ruland, W. *Acta Crystallogr.* 1961, **14**, 1180
32 Marvin, D. N. *J. Soc. Dyers Colour.* 1954, **70**, 16
33 Merian, Y., Carbonell, J., Lerch, U. and Sunahuja, V. *J. Soc. Dyers Colour.* 1963, **79**, 505
34 Mitsuishi, Y. and Tonami, H. *Sen-i Gakkaishi* 1963, **19**, 140
35 Dumbleton, J. H., Bell, J. P. and Murayama, T. *J. Appl. Polym. Sci.* 1968, **12**, 2491
36 Warwicker, J. O. *J. Soc. Dyers Colour.* 1972, **88**, 142
37 Gupta, V. B., Kumar, M. and Gulrajani, M. L. *Text. Res. J.* 1975, **45**, 463
38 Sakai, T., Miyasaka, K. and Ishikawa, K. *Sen-i Gakkaishi* 1978, **34**, T-475
39 Sakaguchi, N., Oda, T., Nakai, A. and Kawai, H. *Sen-i Gakkaishi* 1977, **33**, 499
40 Bonart, R. *Kolloid-Z. Z. Polym.* 1966, **1**, 213
41 Wunderlich, B. and Grebowicz, G. *Adv. Polym. Sci.* 1984, **60/61**, 1
42 Ruland, W. *Kolloid-Z. Z. Polym.* 1977, **255**, 29
43 Fakirov, S., Fischer, E. W. and Schmidt, G. *Makromol. Chem.* 1975, **176**, 2459
44 Huisman, R. and Heuvel, H. M. *J. Appl. Polym. Sci.* 1978, **22**, 943
45 Kavesh, S. and Schults, J. M. *J. Polym. Sci. (A-2)* 1971, **9**, 85
46 Hatakeyama, T. and Hatakeyama, H. *Sen-i Gakkaishi* 1983, **39**, T-461
47 Ishida, Y., Yamafuji, K., Ito, H. and Takayanagi, M. *Kolloid-Z. Z. Polym.* 1962, **184**, 97
48 Yamafuji, K. and Ito, H. *Kolloid-Z. Z. Polym.* 1961, **183**, 15